



**Politecnico
di Torino**

Alfa Romeo MiTo CFD Simulation: RRS OFF

s346643 Maurizio Pio Vergara

Contents

1	Objective	3
2	Methodology	3
3	Mesh Generation and Refinement	4
3.1	Surface and Volume Mesh	4
3.2	Mesh refinements and Boundary conditions	4
4	Post-processing	7
5	Conclusion	11

1 Objective

The aim of this project is to evaluate the aerodynamic performance of the Alfa Romeo MiTo using Computational Fluid Dynamics (CFD) analysis. The specific objectives include:

- Gaining an understanding of the CFD workflow.
- Learning how to set up and run simulations in StarCCM+ software.
- Extracting and analyzing aerodynamic coefficients, specifically drag (C_D) and lift (C_L).
- Comparing simulation results to experimental data and proposing potential methodological improvements.

2 Methodology

The analysis is conducted in the following key stages:

Pre-Processing:

- **Geometry Import:** Import the provided geometry file (*Mito-half-ex1.inp*) and ensure the model is water-tight and free of penetrations or triple edges.
- **Mesh Generation:** Create surface and volume meshes with appropriate refinement for critical regions such as boundary layers and wake zones using automated and custom controls.
- **Boundary Conditions:** Define inlet velocity, outlet pressure, and other physical constraints to replicate wind tunnel conditions.

Simulation Setup:

- **Physics Definition:** Configure a steady-state RANS approach with a $k - \varepsilon$ turbulence model.
- **Solver Configuration:** Optimize numerical schemes, relaxation factors, and stopping criteria for convergence.
- **Execution:** Run simulations in parallel using 4 cores and monitor force coefficients during computation.

Post-Processing:

- Visualize flow fields, pressure, and velocity distributions using scalar displays, streamline visualizations, and iso-surfaces.
- Analyze and export force coefficient histories and other metrics.
- Compare simulation results with experimental data to validate findings.

Test Conditions:

- Current production vehicle
- Closed air intake
- $140 \text{ Km/h} = 38.89 \text{ m/s}$
- EADE ride height
- RRS OFF

3 Mesh Generation and Refinement

In this simulation, the mesh setup was a critical step to ensure accurate results while balancing computational efficiency. The meshing process involved both surface and volume mesh refinement, with specific attention to key regions of the Alfa Romeo MiTo geometry and the wind tunnel setup.

3.1 Surface and Volume Mesh

The mesh was generated using an automated meshing operation in StarCCM+, incorporating the following meshing models:

- Surface Remesher: To enhance the quality of the imported surface mesh.
- Polyhedral Mesher: For volume meshing, offering better representation of complex geometries.
- Prism Layer Mesher: To capture boundary layer effects accurately.

Refinements were applied to both the surface and volume meshes to target areas of high gradients, such as the vehicle's wake region, boundary layers, and flow separation zones. In Figure 1 and

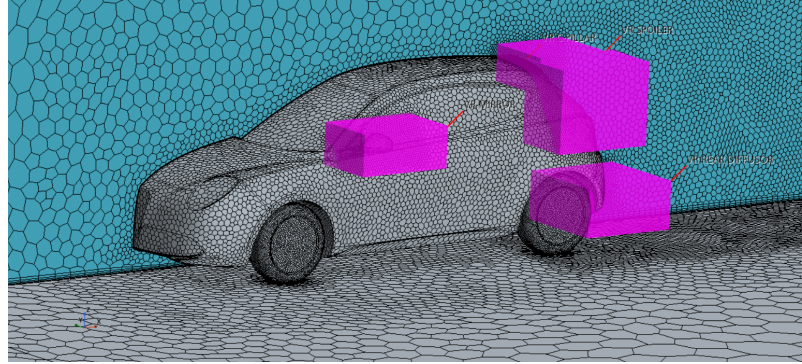


Figure 1: C-pillar, mirror, rear diffusor and spoiler Volume Refinement

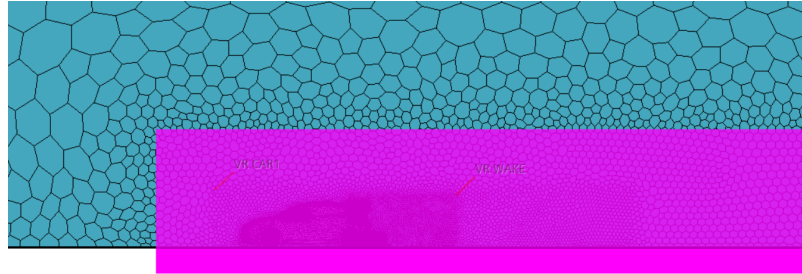


Figure 2: Car and wake Volume Refinement

Figure Figure 2 box shapes of volume mesh are shown.

3.2 Mesh refinements and Boundary conditions

The mesh density and cell sizes were carefully chosen to balance computational efficiency and simulation accuracy. The base cell size was set to 25 mm, serving as the foundation for further refinement. Surface mesh density was controlled with parameters such as a target surface size of 200% and a minimum surface size of 100% of the base size, ensuring a smooth transition with a growth factor of 1.3 to avoid abrupt changes in cell dimensions. Volume mesh refinements were applied to regions with high aerodynamic importance, such as wake zones around the spoiler and mirrors, where smaller cell sizes were used to capture intricate flow details. For boundary conditions and wall refinements, an anisotropic prism layer was implemented near walls to capture high gradients effectively. The near-wall cell thickness was set to 2 mm, with three layers and a total thickness of 10 mm, providing adequate resolution for boundary layer analysis. On the wind tunnel floor, larger cell sizes were used to optimize computational resources, with target and

minimum surface sizes set to 2500% and 250% of the base size, respectively. The prism layers on the floor were further refined with a near-wall thickness of 4 mm, five layers, and a total thickness of 50 mm, ensuring proper resolution of floor interactions with the flow. Additionally, finer surface and volume meshes were applied to key aerodynamic surfaces such as the upper body, mirrors, and spoiler, and wake regions behind the vehicle were refined to capture flow separation and vortex dynamics accurately. This meshing strategy provided a robust foundation for precise and reliable CFD analysis. Mesh cells are shown in Figure 3, 4, 5 and 6.

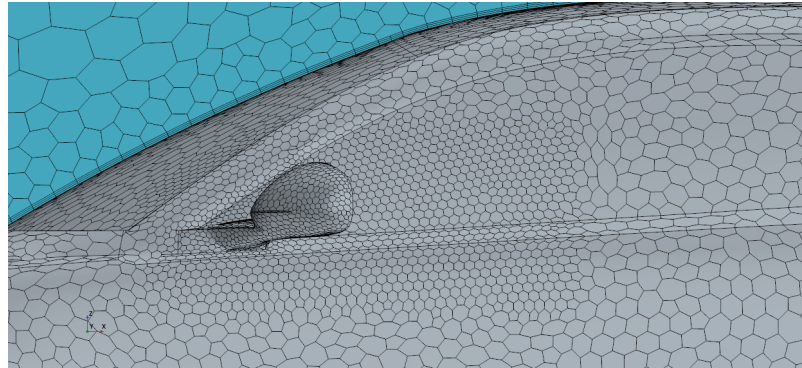


Figure 3: Mirror surface mesh

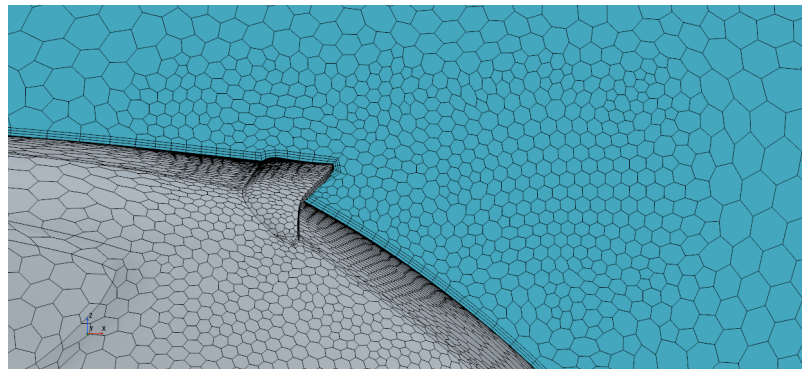


Figure 4: Spoiler and boundary layer surface mesh

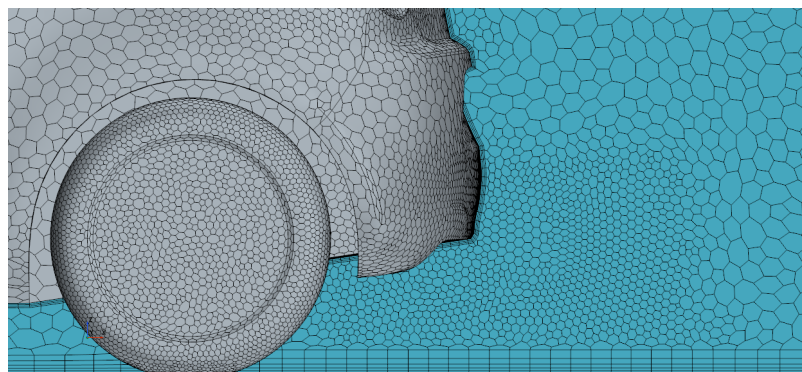


Figure 5: Rear diffusor surface mesh

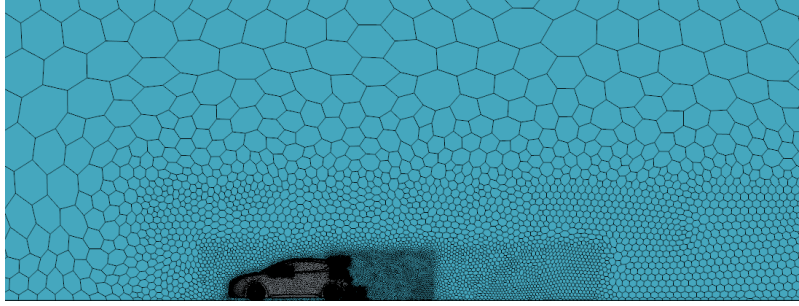


Figure 6: Surfaces meshes of the simulation

In the simulation, plane sections were generated to provide detailed insights into the flow field characteristics around the vehicle. These sections were created by defining cutting planes through the computational domain, enabling the visualization of various flow parameters such as velocity magnitude, pressure distribution, and turbulence intensity. The use of plane sections proved particularly valuable for analyzing critical regions, including the wake behind the vehicle, boundary layer development, and areas of flow separation. By slicing through the flow field, these sections revealed the underlying aerodynamic behavior that is not easily observable from external perspectives.

For this analysis, plane sections were positioned strategically in regions of interest, such as the symmetry plane of the vehicle and transverse planes in the wake region. These visualizations were used to identify key flow features, including shear layers, vortices, and pressure gradients, which are crucial for evaluating the aerodynamic performance of the Alfa Romeo MiTo.

The following images highlight the effectiveness of the meshing strategy and boundary conditions while providing a clear depiction of the aerodynamic phenomena under investigation.

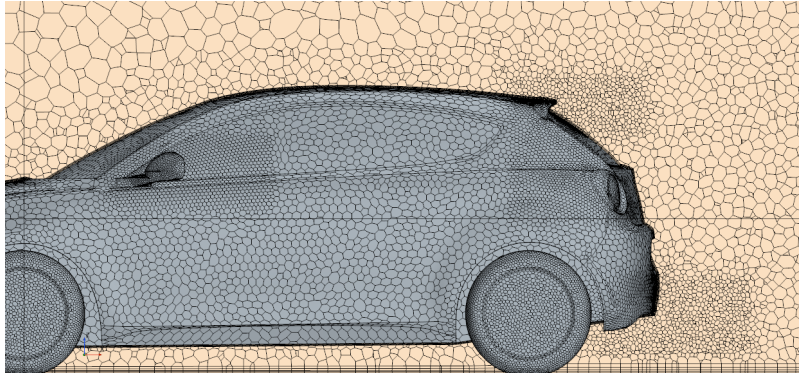


Figure 7: Plane section Y

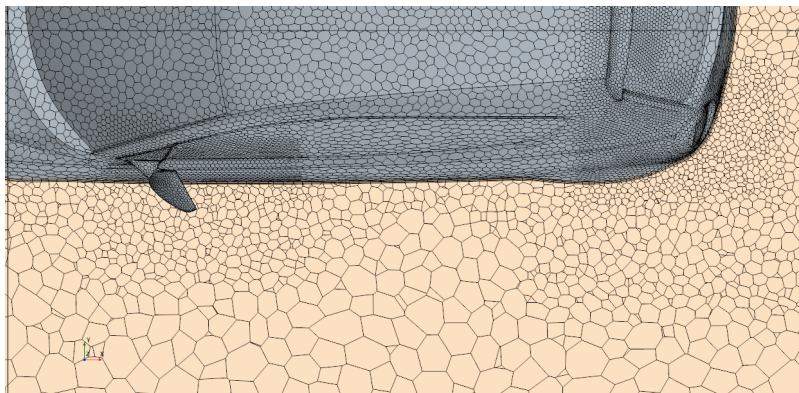


Figure 8: Plane section Z

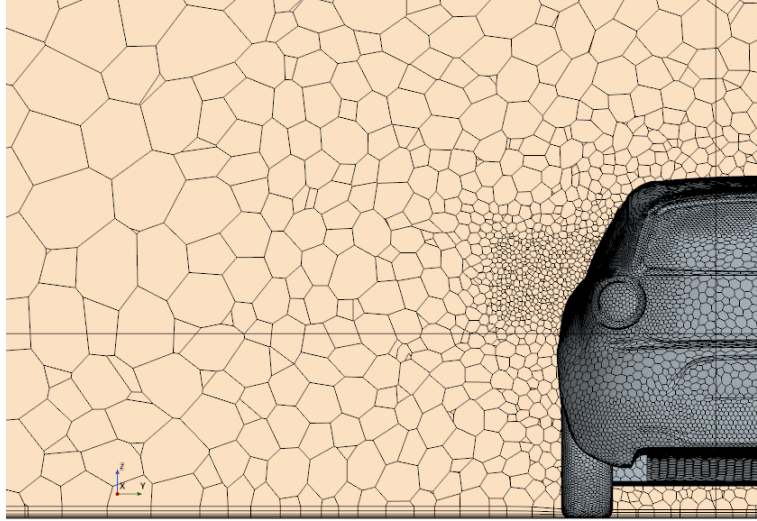


Figure 9: Plane section X

4 Post-processing

The following sections present the setup of the simulation and the results obtained, including the aerodynamic coefficients of drag (C_D) and lift (C_L), as well as the residuals. Drag and lift coefficients are key indicators of the aerodynamic performance of the Alfa Romeo MiTo, reflecting the resistance to motion and the vertical forces acting on the vehicle. Residuals, on the other hand, are numerical indicators of the simulation's convergence; they measure the difference between successive iterations in the solution process. Low residual values signify that the solution has stabilized, ensuring the reliability of the results. These elements provide a comprehensive overview of the vehicle's aerodynamic characteristics and the accuracy of the computational model. In Figure 10 is shown the adopted physics setup for the simulation.

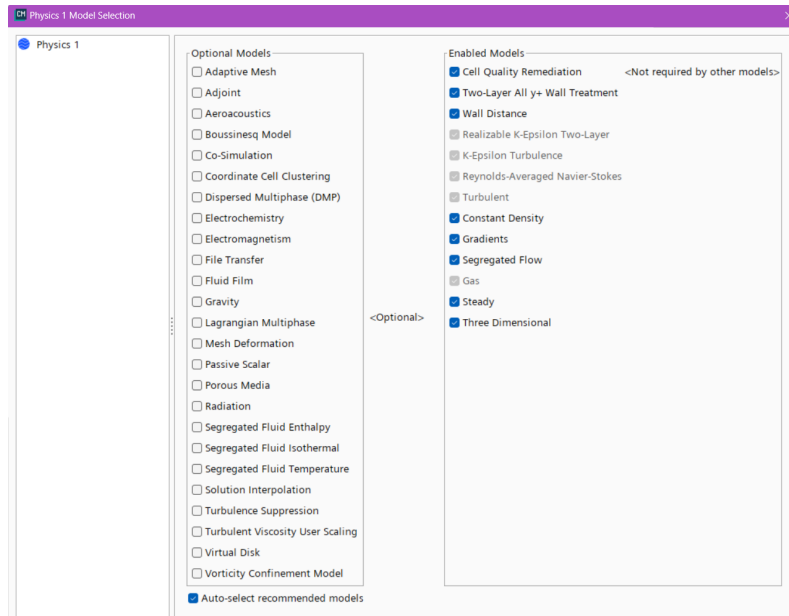


Figure 10: Physics setup

The following figures display the coefficients results:

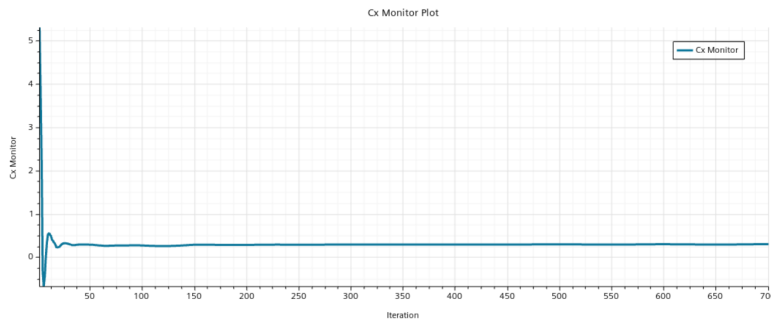


Figure 11: Drag coefficient

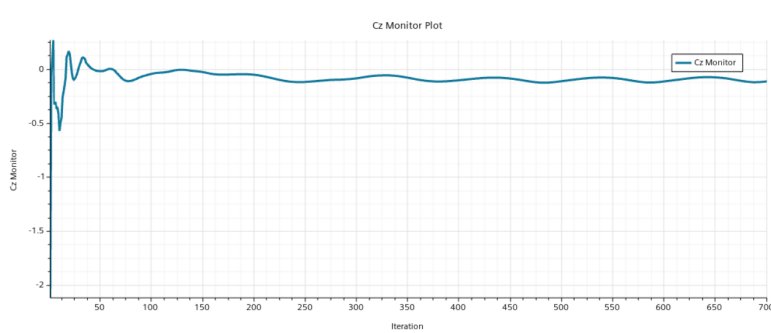


Figure 12: Lift coefficient

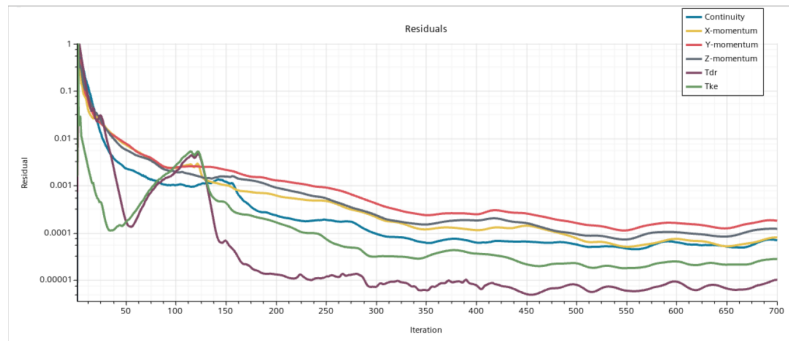


Figure 13: Residuals

Residuals are approximately 3 to 4 orders of magnitude below those of the first iterative solution, indicating that the solution is reliable. The drag coefficient is $C_x = 0.299$. The difference from the experimental value can be attributed to factors such as the flat underbody simulation and the *Rolling Road System* being turned off.

In Figure 14 the drag coefficient development is shown. This plot is useful for understanding where drag is generated or recovered.

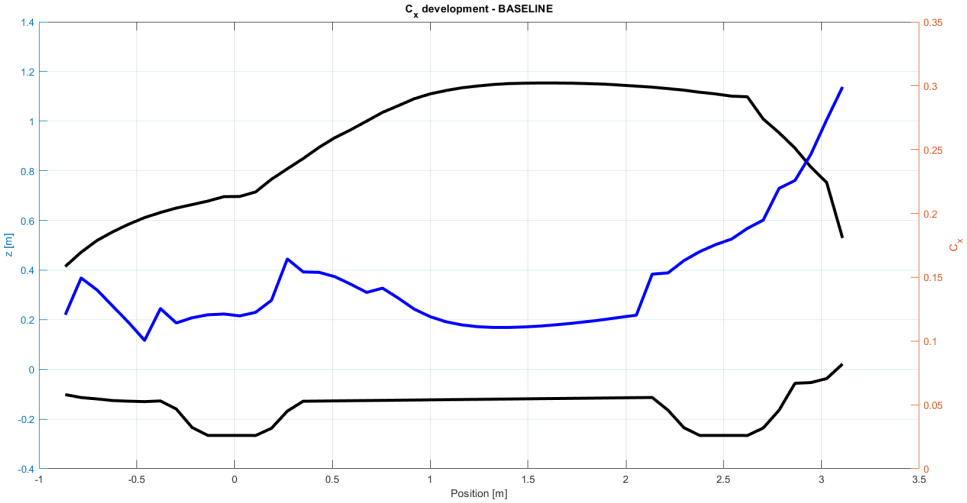


Figure 14: Drag coefficient development

Most of the drag is recovered in the central area of the car, while the most critical area is the rear, where drag increases significantly due to flow separation and turbulence. The rear side of the vehicle is the most important part to design. Generation and recovery of drag can also be compared to other factors such as *Pressure Coefficient*, *Skin Friction Coefficient*, *Velocity Magnitude*, *Streamlines*, and *Iso-surfaces*, which can be obtained through the post-processing workflow.

The **post-processing** phase of the simulation focuses on evaluating key aerodynamic parameters and visualizing flow behaviors around the Alfa Romeo MiTo. Several metrics and techniques were employed to analyze the results in detail:

- **Pressure Coefficient (C_p):** This parameter was used to assess the pressure distribution on the vehicle's surface, identifying regions contributing to drag and lift generation, as well as areas of flow separation.
- **Skin Friction Coefficient:** By analyzing the distribution of skin friction, it was possible to detect shear forces along the surface, highlighting regions with boundary layer separation and wake formation.
- **Velocity Magnitude:** Visualizations of velocity fields provided insights into flow acceleration, deceleration, and wake characteristics, helping to evaluate aerodynamic efficiency.
- **Streamlines:** These were utilized to trace the flow direction and identify vortex structures and flow paths, particularly in the wake and around complex geometries such as mirrors and spoilers.
- **Iso-surfaces:** Iso-surfaces of total pressure coefficients were generated to visualize wake regions and low-pressure zones, offering a three-dimensional representation of aerodynamic phenomena.

These post-processing techniques not only facilitated a deeper understanding of the vehicle's aerodynamic behavior but also provided essential visual evidence to validate and discuss the simulation results.



Figure 15: Pressure coefficient and Velocity magnitude

Simcenter STAR-CCM+

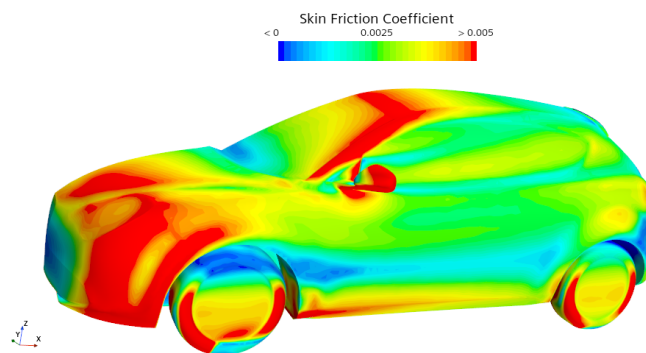


Figure 16: Skin friction coefficient

It is noticeable that there is a well-attached flow on the front bumper, while a separated flow occurs at the front of the vehicle and along the entire rear bumper. In Figure 17 and Figure 18, the streamlines of the velocity magnitude are displayed. Velocity is around 0 m/s at the front wheel and on the rear bumper, while it is maximum on the vehicle's side, where the flow is well-attached.

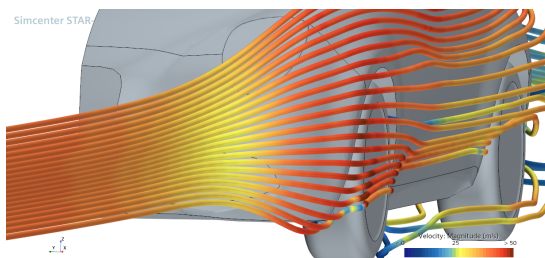


Figure 17: Streamlines on the front wheel

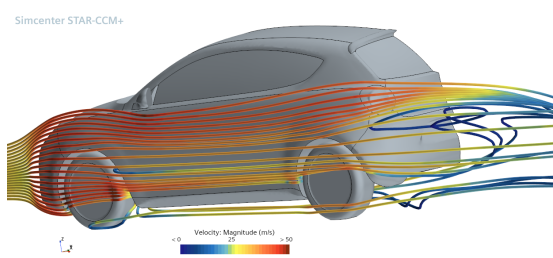


Figure 18: Streamlines on the vehicle's side

The **Iso-surface** is used to visualize the total pressure coefficient on the car and, in detail, where the flow detaches from the vehicle. In Figure 19 and Figure 20, the results are reported.

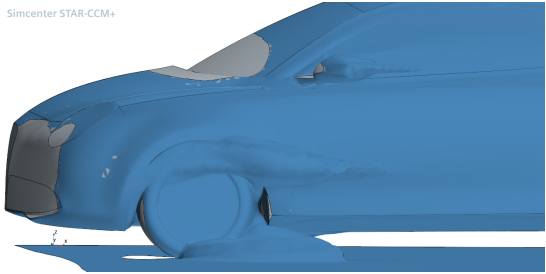


Figure 19: Iso-surface on the front side vehicle

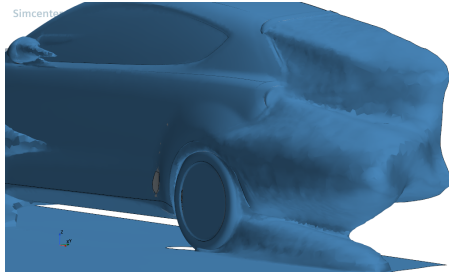


Figure 20: Iso-surface on the rear side vehicle

5 Conclusion

In conclusion, the flow field detaches around the mirrors, wheels, and rear bumper. These are the most critical areas for aerodynamic performance. To obtain better results that are more similar to experimental data, the RRS could be simulated. To do so, a moving ground surface is created under the vehicle using a moving wall or sliding mesh to represent road motion. The vehicle's speed is set, and appropriate boundary conditions for airflow are applied. The moving ground is set to match the vehicle's speed, and the flow around the vehicle is simulated with the ground moving beneath it.



**Politecnico
di Torino**

Alfa Romeo MiTo CFD Simulation: Comparison of the vehicle with/without spats

s346643 Maurizio Pio Vergara

Contents

1	Objective	3
2	Geometry and Mesh Comparison	3
3	Drag Analysis	3
3.1	Simulated RRS	4
4	Flow Characteristics Comparison	4
4.1	Pressure Coefficient	4
4.2	Skin Friction Coefficient	5
4.3	Total Pressure Coefficient (Iso-surface)	6
4.4	Velocity Magnitude and Streamlines	7
4.5	Velocity Sections	7
5	Conclusion	8

1 Objective

This report presents a comparative analysis of the aerodynamic performance of two vehicle models: one equipped with spats and the other without. Computational Fluid Dynamics (CFD) simulations are utilized to investigate differences in drag, pressure coefficient, skin friction coefficient, velocity magnitude, and total pressure coefficient. The study aims to identify the impact of spats on the overall aerodynamic performance of the vehicle.

2 Geometry and Mesh Comparison

A comparison of the geometries and computational meshes of the two models is presented in Figures 1, 2, 3 and 4.

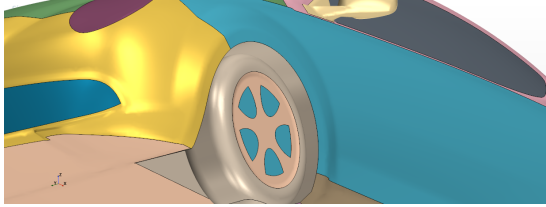


Figure 1: Vehicle geometry without spats.

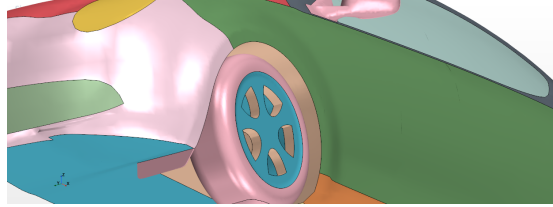


Figure 2: Vehicle geometry with spats.

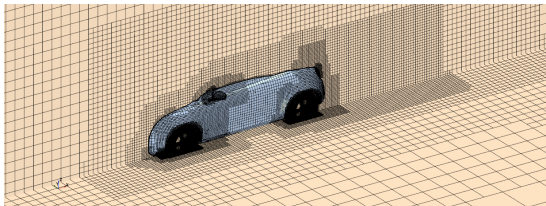


Figure 3: Vehicle mesh without spats.

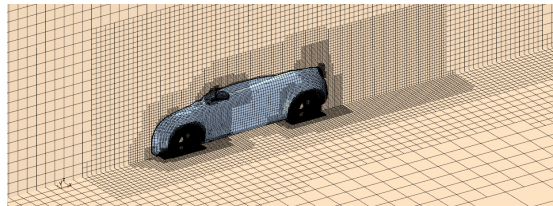


Figure 4: Vehicle mesh with spats.

3 Drag Analysis

The drag coefficient (C_D) along the vehicle's length is compared for the two configurations. Figures 5 and 6 illustrate the respective results.

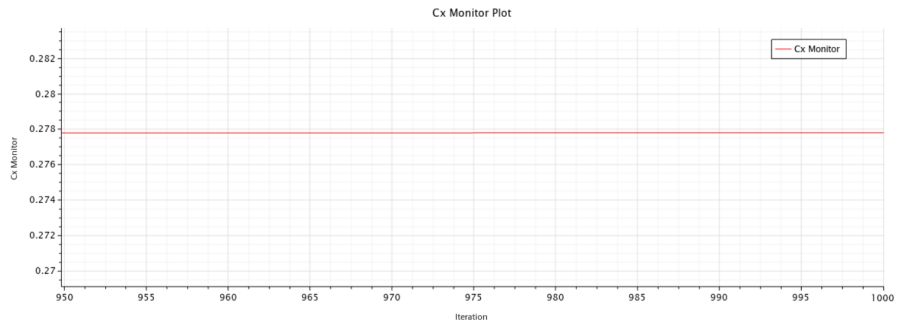


Figure 5: Drag coefficient distribution for the vehicle without spats.

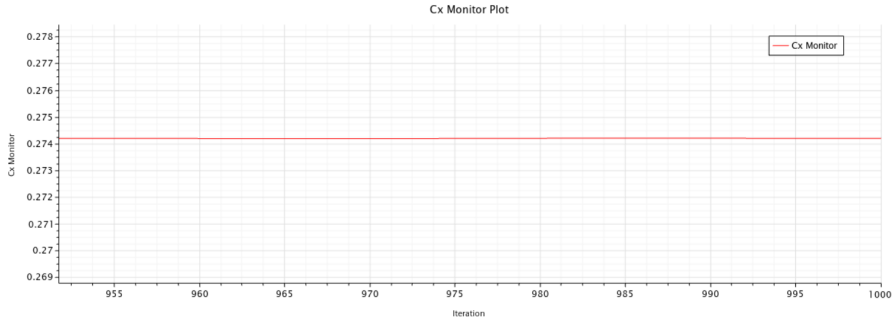


Figure 6: Drag coefficient distribution for the vehicle with spats.

The results show that the model with spats exhibits a lower drag coefficient, indicating improved aerodynamic efficiency.

The model with spats exhibits a lower drag coefficient due to improved aerodynamic efficiency. Spats reduce turbulence around the wheels by enclosing them, leading to smoother airflow and minimizing wheel wake effects. They also enhance flow attachment along the vehicle, decreasing pressure drag by reducing separation zones and stagnation regions. Additionally, spats lower the vehicle's effective frontal area and mitigate interference drag between the wheel wake and the body. These improvements streamline the flow, optimize pressure distribution, and reduce turbulence, as supported by CFD analyses of pressure coefficients, velocity streamlines, and skin friction plots.

3.1 Simulated RRS

RRS is simulated by applying a tangential velocity to the wheel, ensuring that the contact point with the ground has a velocity of $v = 38.89 \text{ m/s}$, while the furthest point from the ground has a velocity of $v = -38.89 \text{ m/s}$, as depicted in Figures 7 and 8.

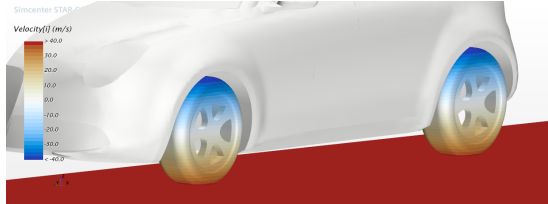


Figure 7: RRS - Model without spats.

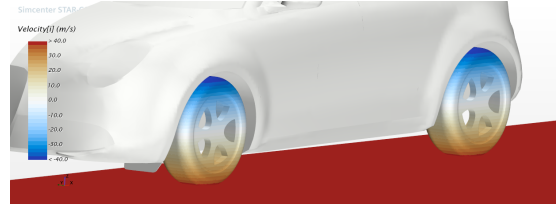


Figure 8: RRS - Model with spats.

4 Flow Characteristics Comparison

4.1 Pressure Coefficient

Comparisons of the pressure coefficient distributions on the vehicle surfaces are provided. Further visualizations highlight the differences in pressure fields around the models.

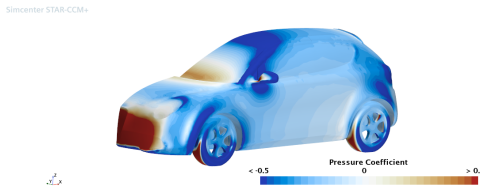


Figure 9: C_P - Model without spats.

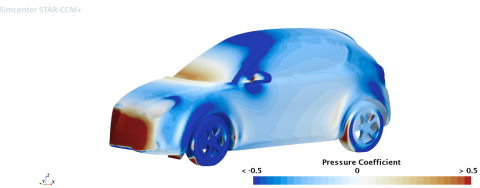


Figure 10: C_P - Model with spats.

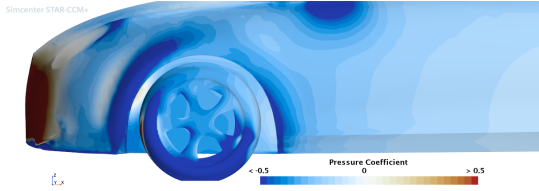


Figure 11: C_P on front wheel - Model without spats.

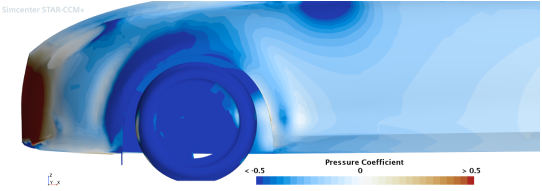


Figure 12: C_P on front wheel - Model with spats.

The pressure coefficient distributions on the vehicle's surface for the configurations with and without spats reveal distinct aerodynamic differences.

In the model without spats, higher-pressure zones, indicated by warmer colors (closer to red), are prominent near the front bumper and around the wheel regions. The absence of spats allows more airflow to interact directly with the wheels, creating increased pressure regions and turbulence. This interaction contributes to a more disturbed airflow, particularly around the lower side of the vehicle.

In the model with spats, the pressure coefficient distribution shows a reduction in high-pressure zones near the wheels. The spats streamline the airflow around the wheels, reducing turbulence and improving aerodynamic efficiency. The smoother transition of airflow along the vehicle's body results in a more uniform pressure distribution, as evidenced by the dominance of cooler colors (blue tones) across the surface.

Overall, the addition of spats reduces aerodynamic drag by minimizing high-pressure buildup and smoothing airflow interactions, contributing to better vehicle performance.

4.2 Skin Friction Coefficient

To compare the skin friction coefficient distributions for the models with and without spats, the analysis highlights key differences on the front bumper (Figures 13, 14), rear bumper (Figures 17, 18), and vehicle's sides (Figures 15, 16), along with their implications for flow attachment or detachment.

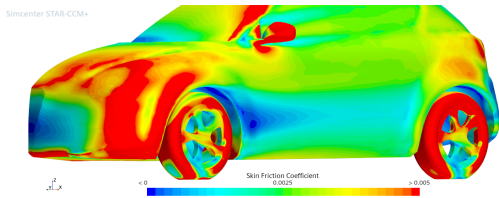


Figure 13: Skin friction on the front - Model without spats.

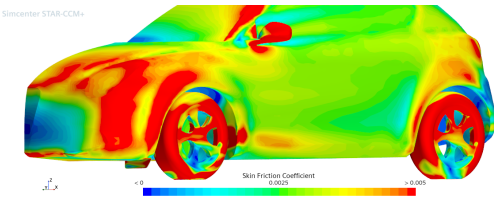


Figure 14: Skin friction on the front - Model with spats.

In the model without spats, the skin friction coefficient is higher in localized areas, particularly near the front bumper, where airflow stagnation and turbulent effects are prominent. Along the vehicle's sides, the absence of spats leads to increased interaction between the airflow and the wheels, creating regions of higher shear stress. On the rear bumper, the coefficient decreases significantly due to flow detachment, resulting in wake formation and increased drag. These patterns indicate a less streamlined airflow, with significant regions of boundary layer separation that increase overall aerodynamic resistance.

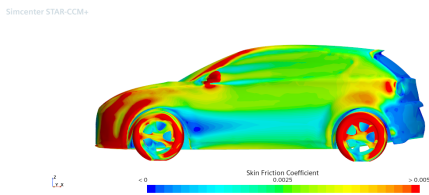


Figure 15: Skin friction on the side - Model without spats.

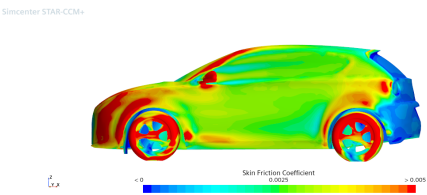


Figure 16: Skin friction on the side - Model with spats.

In contrast, the model with spats exhibits a lower and more uniform skin friction coefficient, especially along the vehicle's sides and rear bumper. The presence of spats smooths the airflow around the wheels, reducing localized shear stress and maintaining flow attachment for a longer distance along the vehicle's body. On the front bumper, the distribution is slightly more uniform, with reduced shear stress peaks compared to the no-spats configuration. At the rear, the smoother transition and delayed flow detachment minimize the wake region and improve aerodynamic performance.

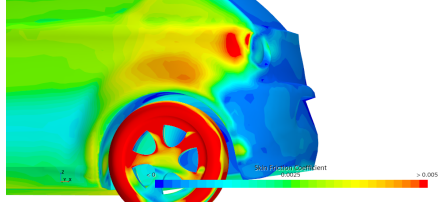


Figure 17: Skin friction on the rear - Model without spats.

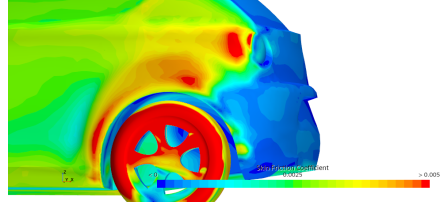


Figure 18: Skin friction on the rear - Model with spats.

The addition of spats promotes better flow attachment along the sides and rear of the vehicle, reducing drag and turbulence. This results in an overall improvement in aerodynamic efficiency, as the streamlined flow reduces energy losses associated with shear stress and wake formation.

4.3 Total Pressure Coefficient (Iso-surface)

The analysis of total pressure coefficient iso-surfaces highlights key differences between the Alfa Romeo MiTo with and without spats. With spats, the flow detaches more noticeably along the lower profile of the vehicle, particularly near the underbody and rear, resulting in extended separation regions. While the spats effectively reduce turbulence around the wheels by redirecting the airflow, they induce greater flow detachment downstream, influencing the wake structure and pressure recovery.

In contrast, the configuration without spats exhibits better flow attachment along the lower profile but generates higher turbulence near the wheel arches. This leads to broader wake regions and increased drag due to unorganized flow interactions with the wheels. The spats, therefore, improve local aerodynamic efficiency around the wheels but alter the overall flow behavior along the vehicle's sides and rear, reflecting a trade-off in performance.

The results are shown in the following Figures:

Simcenter STAR-CCM+

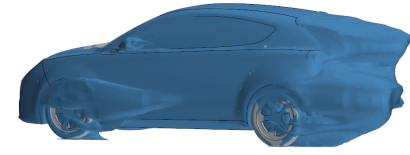


Figure 19: C_{TP} - Model without spats.

Simcenter STAR-CCM+

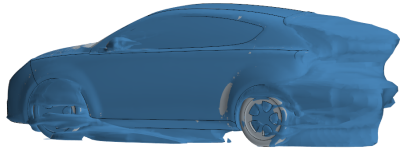


Figure 20: C_{TP} - Model with spats.

Simcenter STAR-CCM+

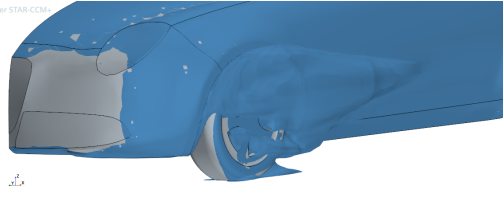


Figure 21: C_{TP} on the front - Model without spats.

Simcenter STAR-CCM+

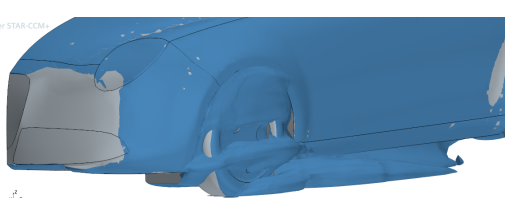


Figure 22: C_{TP} on the front - Model with spats.

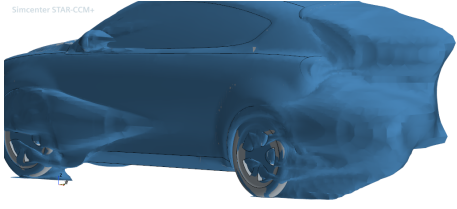


Figure 23: C_{TP} on the rear - Model without spats.

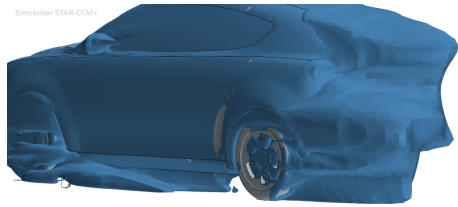


Figure 24: C_{TP} on the rear - Model with spats.

4.4 Velocity Magnitude and Streamlines

Streamline plots and velocity magnitude visualizations are utilized to compare flow patterns. In the configuration with spats, the streamlines show a smoother deflection around the front wheels, with reduced turbulence and flow separation in the wheel region. The spats help guide the airflow more efficiently, minimizing the disturbance caused by the rotating wheels. However, the introduction of spats also leads to a more significant deflection of the flow under the vehicle, causing higher separation along the underbody and at the rear. This results in an expanded low-velocity wake downstream, which can affect pressure recovery and overall drag.

Conversely, the configuration without spats exhibits more disorganized streamlines near the front wheels due to direct interaction between the freestream and the rotating wheels. This leads to higher turbulence and velocity gradients in these regions. However, the flow under the vehicle and around the lower profile remains more attached, with less severe wake formation at the rear. The absence of spats allows the flow to follow a more continuous path beneath the car, albeit with increased disturbance near the wheels.

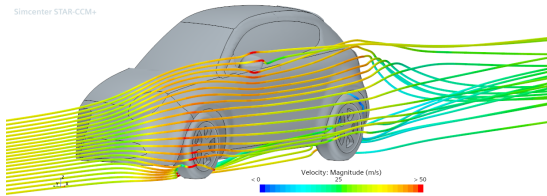


Figure 25: Streamline on the front - Model without spats.

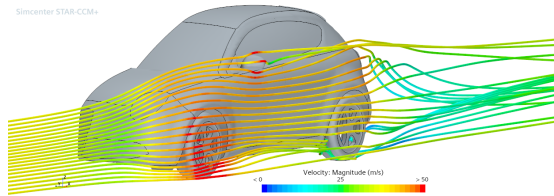


Figure 26: Streamline on the front - Model with spats.

The spats, therefore, effectively streamline the flow around the wheels, reducing localized turbulence, but they also alter the overall flow pattern beneath the vehicle, leading to increased separation in other areas. This highlights the trade-off between localized improvements in aerodynamic efficiency and potential downstream effects on wake behavior and drag.

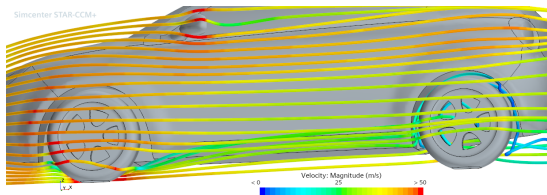


Figure 27: Streamline on the wheels - Model without spats.

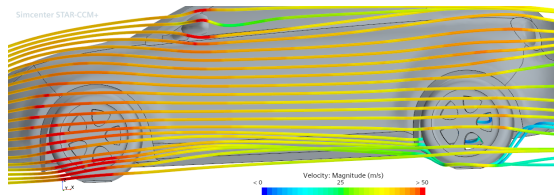


Figure 28: Streamline on the wheels - Model with spats.

4.5 Velocity Sections

Cross-sectional velocity contours are analyzed to observe flow development along the vehicle's length. In the configuration without spats, the velocity field shows higher intensity near the front wheel region, indicating stronger flow acceleration and turbulence caused by the direct interaction of freestream air with the rotating wheels. The absence of spats leads to greater flow disruption around the wheel arches, resulting in higher local velocity gradients. This configuration also exhibits a less smooth velocity distribution in the underbody region, where air interacts directly with exposed surfaces.



Figure 29: YZ velocity section - Model without spats.



Figure 30: YZ velocity section - Model with spats.

Conversely, in the with spats configuration, the velocity contours indicate a more organized and controlled airflow around the lower front section of the vehicle, as shown in Figure 32. The spats act to streamline the flow near the wheels, reducing the high-velocity regions and mitigating turbulence in this area. The flow beneath the vehicle appears more uniform, with lower velocity gradients immediately adjacent to the wheel arches. This smoother distribution helps minimize aerodynamic disturbances and may contribute to improved local flow conditions.

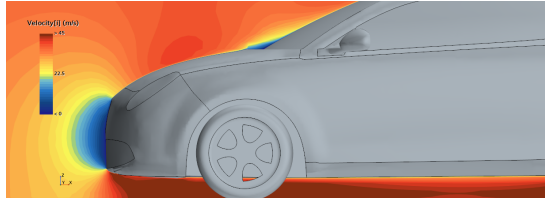


Figure 31: XZ velocity section - Model without spats.

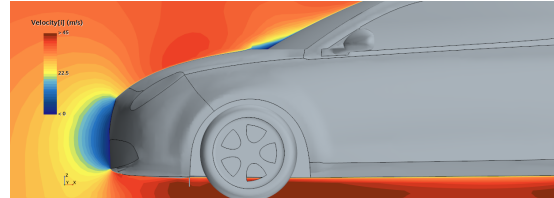


Figure 32: XZ velocity section - Model with spats.

Overall, the spats enhance the flow uniformity near the wheels and reduce localized high-velocity zones, improving the aerodynamic efficiency of the lower frontal region. However, this also redistributes the flow, potentially affecting the pressure recovery and flow separation in downstream regions of the vehicle.

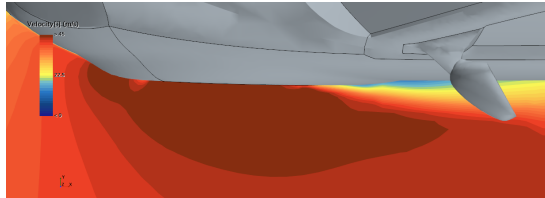


Figure 33: XY velocity section on the front wheel - Model without spats.

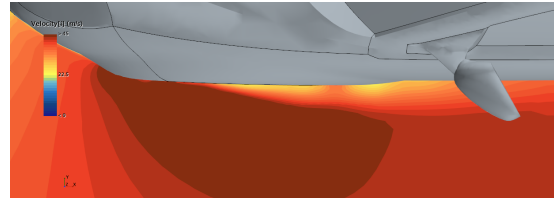


Figure 34: XY velocity section on the front wheel - Model with spats.

5 Conclusion

The inclusion of **spats** reduces the overall drag coefficient ($\Delta C_D = -0.004$), demonstrating their effectiveness in improving aerodynamic performance. Although the drag coefficient is higher in the front wheel area in the model with spats, it achieves a lower overall C_D , demonstrating significant drag coefficient recovery. The following figures illustrate the drag distribution along the vehicle's profile, as well as the lift and residuals, highlighting the reliability of the simulations. Both configurations exhibit residuals several orders of magnitude lower than at the start of the simulation, confirming the numerical convergence of the results. For the no-spats configuration, the lift force is lower in absolute magnitude, indicating a reduced downforce acting on the vehicle. This reduction in downforce is generally detrimental to vehicle performance, as it decreases the normal force exerted on the tires, thereby reducing grip and compromising stability, particularly at higher speeds. It should be noted that the lift coefficient values are not very reliable and may not reflect reality, as the simulations were carried out using two flat underbody models, which are therefore different from the actual model.

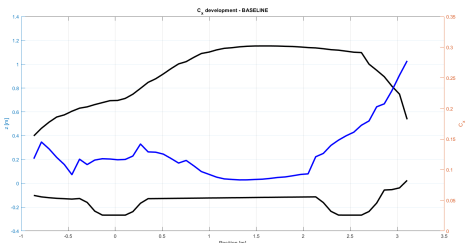


Figure 35: Drag distribution along the vehicle's profile - without spats.

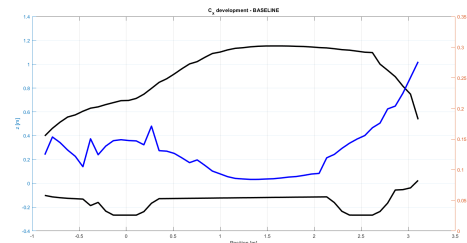


Figure 36: Drag distribution along the vehicle's profile - with spats.

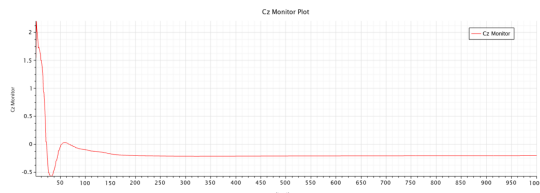


Figure 37: Lift coefficient - without spats.



Figure 38: Lift coefficient - with spats.

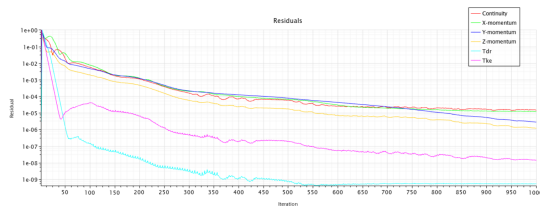


Figure 39: Residuals - without spats.

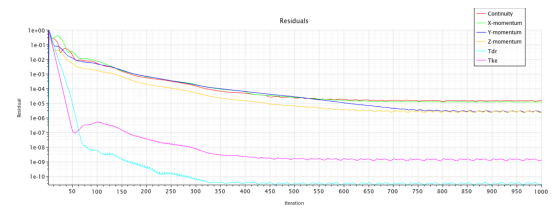


Figure 40: Residuals - with spats.